LAWRENCE
LIVERMORE
NATIONAL
LABORATORY

LLNL-JRNL-401946

In-Situ Monitoring of the Microstructure of TATB-based Explosive Formulations During Temperature Cycling using Ultra-small Angle X-ray Scattering

T. M. Willey, D. M. Hoffman, T. van Buuren, L. Lauderbach, J. Ilavsky, R. H. Gee, A. Maiti, G. Overturf, L. Fried

March 4, 2008

Propellants, Explosives, Pyrotechnics

Disclaimer

In-Situ Monitoring of the Microstructure of TATB-based Explosive Formulations During Temperature Cycling Using Ultra-small Angle X-ray Scattering

Trevor M. Willey[1]*, D. Mark Hoffman[1], T. van Buuren[1], Lisa Lauderbach[1], Jan Ilavsky[2], Richard H. Gee[1], Amitesh Maiti[1], George Overturf[1], Laurence E. Fried[1]

Lawrence Livermore National Laboratory, 7000 East Avenue, Livermore CA 94550

Advanced Photon Source, Argonne National Laboratory, Argonne, IL

(Received: May ??, 2008, revised ??, 2008)

DOI: ???

Abstract

TATB (1,3,5 triamino-2,4,6-trinitrobenzene), an extremely insensitive explosive, is used both in plastic-bonded explosives (PBXs) and as an ultra-fine pressed powder (UFTATB). With both PBXs and UFTATB, an irreversible expansion occurs with temperature cycling known as ratchet growth. In TATB-based explosives using Kel-F 800 as binder (LX-17 and PBX-9502), additional voids, sizes hundreds of nanometers to a few microns account for much of the volume expansion caused by temperature cycling. These voids are in the predicted size regime for hot-spot formation during ignition and detonation, and thus an experimental measure of these voids is important feedback for hot-spot theory and for determining the relationship between void size distributions and detonation properties. Also, understanding the mechanism of ratchet growth allows future choice of explosive/binder mixtures to minimize these types of changes to explosives, further extending PBX shelf life. This paper presents the void size distributions of LX-17, UFTATB, and PBXs using commercially available Cytop M, Cytop A, and Hyflon AD60 binders during temperature cycling between -55º C and 70º C. These void size distributions are derived from ultra-small angle x-ray scattering (USAXS), a technique sensitive to structures from about 10 nm to about 2 μm. Structures with these sizes do not appreciably change in UFTATB, indicating voids or cracks larger than a few microns appear in UFTATB during temperature cycling. Compared to Kel-F 800 binders, Cytop M and Cytop A show relatively small increases in void volume from 0.9% to 1.3% and 0.6% to 1.1%, respectively, while Hyflon fails to prevent irreversible volume expansion (1.2% to 4.6%). Computational mesoscale models of ratchet growth and binder wetting and adhesion properties point to mechanisms of ratchet growth, and are discussed in combination with the experimental results.

Keywords: TATB, LX-17, Kel F-800, USAXS, UFTATB, ratchet growth, temperature cycling

LLNL-JRNL-401946

---

* Corresponding author; e-mail: willey1@llnl.gov

1 Introduction

TATB (1,3,5 triamino-2,4,6-trinitrobenzene), an extremely insensitive explosive, is used both in plastically-bonded explosives (PBXs) and as an ultra-fine pressed powder (UFTATB). The most common PBX's use Kel-F 800, a commercial fluoropolymer, in formulations known as LX-17 (92.5% TATB / 7.5% binder) and PBX-9502 (95% TATB / 5% binder.) PBXs allow for the production of solid explosives that can be pressed or machined into desired shapes. Several additional fluoropolymer binders for TATB have recently been proposed based on wetting and adhesion properties with TATB[1]. Three of these fluoropolymers, Cytop A, Cytop M, and Hyflon AD60 are tested in this work as binders for comparison with LX-17 and the binder-less UFTATB.

In TATB-based explosives using Kel-F 800 binder, an irreversible expansion occurs upon thermal cycling that is a function of temperature and time[2, 3]. This irreversible expansion is referred to as *ratchet growth*. Both experiment and theory show that TATB crystals expand with increasing temperature, primarily along the axis perpendicular to the plane of the molecule[4]. Molecular dynamics modelling predicts that this expansion should produce about a 3% increase in total volume[5]. These simulations also predict that in single crystallites, the expansion should be reversible. The experimentally observed irreversible expansion indicates that temperature cycling produces permanent damage, possibly by the anisotropic expansion of randomly oriented TATB crystallites. Further, binders with higher glass transition temperatures (Tg) have previously been correlated with the suppression of ratchet growth[6, 7].

Temperature cycling and the resulting change in density affect the detonation velocity[8-10] and shock sensitivity[11] in these highly insensitive explosives. These differences are presumably due to the voids created or altered during ratchet growth. Hot-spot models predict that voids on the order of 100 nm to 1 μm affect detonation properties[12-14]. As these voids are in the predicted size regime for hot-spot formation during initiation and detonation, experimental determination of void size distributions is essential feedback to both hot-spot theory and to experimentally determine the relationship between void size-distributions and detonation properties.

Previous results using ultra-small angle x-ray scattering (USAXS) obtained void size distributions for two formulations of TATB-based polymer bound explosives. First, voids were characterized in pristine, pressed samples. Then, changes in the void size distribution were measured after severe thermal cycling and ratchet growth. LX-17 and PBX-9502 have bimodal log-normal void-volume size distributions; for voids of interest, these distributions have maximums at about 100-200 nm. These distributions shift toward larger average void size and higher void concentration with thermal cycling[15]. In this particular study, the total void volume derived from the USAXS data, from 2 nm to about 2 microns, is for LX-17 and PBX-9502, 1.5% and 1.6% respectively, and grows to 2.4% and 2.5% after thermal cycling. Based on the deviation from a 1:1 correlation with density, before ratchet growth, about 75-80% of the

voids are accounted for with USAXS, while after ratchet growth, about 65% of the voids are accounted for, indicating the existence and creation of voids with dimensions larger than a few microns.

To further deduce the mechanism for ratchet growth, this paper investigates the size distributions of voids in various TATB-based explosives using USAXS during the temperature cycling from approximately -55º C to 70º C. These in-situ measurements are performed on LX-17, UFTATB, and three PBXs incorporating fluoropolymer binders proposed for TATB (Cytop-M, Cytop-A, and Hyflon)[1]. These three have higher glass-transition temperatures than Kel-F 800 materials but vary in TATB wetting[1], and can thus isolate how this parameter affects ratchet growth. Collection during the actual temperature cycle allows dynamically measuring changes to voids, and at what times during the cycle changes are occurring. To understand the mechanisms for ratchet growth, computation of binder/TATB wetting[1] and mesoscale models of ratchet growth[16, 17] are compared to the experimental data.

2 Experimental

2.1 Sample Preparation

All TATB/binder mixtures consisted of 92.5% wet-aminated TATB and 7.5% binder, by weight. Disks of about 1 cm in diameter and 0.8 mm in thickness were pressed 3 times at 30 K PSI for 5 minutes. LX-17 samples (92.5% TATB / 7.5% Kel-F 800), from lots C-146 and C-063, were soaked at 105º C for 10 minutes before pressing. To investigate ratchet growth using formulations with new, alternate binders of Cytop M™, Cytop A™, and Hyflon AD60™ were pressed into 0.8mm thick disks, at 120º C, 120º C, and 130º C respectively. These were pressed 3 times at 30 K PSI for 3 minutes each. Ultra-fine TATB was also pressed into these thin disks, at room temperature. This particular binder-less explosive consists of TATB particles/crystallites nominally smaller than about 10 μm, with ~ 0.25% polysaccharide coating to promote adhesion between crystallites.

2.2 Techniques

Inhomogeneities in electron density give rise to small angle x-ray scattering. In its simplest form, the scattered intensity is the square of the Fourier Transform of the scattering length density[18, 19]. Systems containing dilute particles with uncorrelated positions and random orientation lead to negligible effects arising from particle-particle correlation, and the scattering is only a function of the form factor, or size and shape of the particles. In this approximation, and for a single population of scatterers, the scattering can be written in the following form[20, 21]:

$$I(q) = |\Delta\rho|^2 \int_0^\infty |F(q,r)|^2 V^2(r) NP(r) dr \qquad (1)$$

In Eq. 1, $q = \frac{4\pi}{\lambda}\sin(\theta)$, where λ is the wavelength of scattered radiation and θ is the scattering half angle. Also, r is the radius size of the scattering particle, $\Delta\rho$ is the scattering contrast (related to the difference in electron density) between the minority and majority phases, $F(q,r)$ is the scattering form factor, $V(r)$ is the volume of the particle, N is the total number of minority phase particles, and $P(r)$ is the probability of having a minority phase particle of size r. Void size-distributions, $V(d/2)NP(d/2)$, as a function of diameter d, are presented in this work.

Voids cause small angle scattering, and are assumed randomly and uniformly dispersed throughout the explosive. The scattering length density differs only slightly for the explosive TATB ($\rho \approx 16.4 \times 10^{10} cm^{-2}$) and its binder (Kel-F 800, Cytop A, Cytop M, and Hyflon all have $\rho \approx 15 \times 10^{10} cm^{-2}$). In contrast, the voids (with $\rho \approx 0\ cm^{-2}$) within the explosive matrix have very different scattering length density and are the primary source of small-angle scattering.

Although a given electron density distribution gives a unique scattering intensity profile according to Eq. 1, the inversion is not unique and requires model assumptions about microstructure. For this study, the voids are modelled using a form factor for spheres and a maximum entropy algorithm calculates size distributions of the voids [21]. This iterative, linear inversion method, which does not require an *a priori* guess as to the shape of the distribution, converges to a unique distribution of sizes for a given form factor by maximizing the configurational entropy subject to fitting the measured scattering profile[20, 22, 23].

The USAXS data were acquired using the UNICAT beam line 32-ID at the Advanced Photon Source, Argonne National Laboratory, Argonne, Illinois, U.S.A.[24-26]. The endstation consists of a Bonse-Hart camera, which can measure scattering vectors (q) from about 10^{-4}Å^{-1} to 1 Å^{-1}. The monochromator was positioned at about 11 keV (1.13 Å or 0.113 nm). Data were processed using the codes developed for use on this USAXS instrument, and included absolute scattering intensity calibration and slit desmearing. The maximum entropy method, implemented in the "Irena" package for SAS data analysis, was used to determine scatterer size distributions [21]. Desmeared data points from 1.5 x 10^{-4} to 5 x 10^{-2} Å^{-1} in q were used for the maximum entropy calculations.

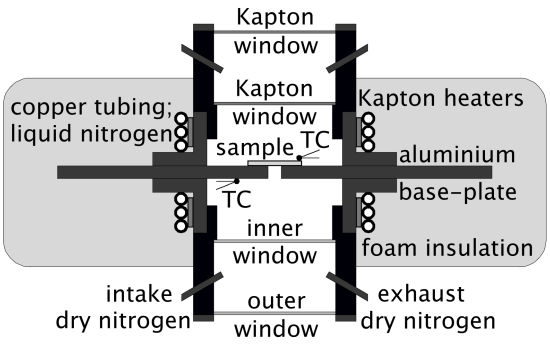

Figure 1: Schematic of the in-situ temperature cycling apparatus. The sample is mounted on an aperture in the aluminum plate; this plate is heated by small Kapton heaters and cooled by liquid nitrogen. Temperature feedback occurs through K-type thermocouples (TC) mounted to the aluminum plate and sample. Warm, dry nitrogen flowing between a set of two Kapton windows on each side of the plate prevents water condensation on the windows and sample during cold cycles. The x-ray beam path is through the center of the figure from bottom to top.

In-situ ratchet growth was accomplished using a custom built cell appropriate for the small-angle x-ray scattering measurements. USAXS is highly sensitive to water droplet formation at surfaces; thus, care must be taken to avoid condensation on the sample or any windows in the path of the scattering x-rays, especially during cold cycles. The cell (see Fig. 1) consists of an aluminum plate insulated from the local environment by foam, plastic, and multiple 7.5 micron-thick Kapton windows along the x-ray path. Small aluminum cylinders attached to each side of this plate are heated by a total of four 1 cm x 10 cm kapton heaters, up to 28V, 20W each (Omega Corp.). These heaters are attached with thermally conductive epoxy for cell heating and temperature control. A single length of ¼" (0.65 cm) O. D. copper tubing, coiled around the outside of these aluminum cylinders and heaters, provides cooling. Liquid nitrogen was delivered to the cell via vacuum-jacket hose (SigmaSystems, Inc.), with an inline solenoid valve for control of liquid flow. Venting of the cold nitrogen from the exhaust end of the cell occurred via a similar vacuum jacket hose.

Samples were mounted with Scotch and/or Kapton tape to the aluminum base-plate. This plate contains multiple sample positions (not shown) with ¼" apertures for x-ray transmission. Thermocouples (K-type, Omega) were attached to both the aluminum plate (with highly thermally conductive epoxy, EPO-TEK H74, Epoxy Technologies) and to the explosive, on the opposite side of the Al plate with Kapton tape. This ensured that during ratchet growth, the specimen was near equilibrium with the aluminum plate. During the ratchet growth cycles, this thermocouple deviated from the Al plate by no more than about 3 degrees C during the most aggressive cooling or heating portions of the temperature cycle. The positions of the USAXS scans on the sample were adjusted at the various temperatures to account for the estimated expansion and contraction of the aluminum plate to probe nearly the same sample volume during each scan.

3 Results and Discussion

3.1 Experimental Results

A representative temperature cycle for the Cytop M, Cytop A, and Hyflon binders is presented in figure 2. These new test formulations were cycled at the same time, resulting in a somewhat slower but more time-efficient cycle: 10 hours for 2.5 cycles. UFTATB and LX-17 were cycled in similar fashion, at a somewhat faster cycle rate: 6 hours for 2.5 cycles in the case of LX-17. USAXS measures scattering in one dimension, using a slit-smeared Bonse-Hart geometry[25-27], and thus scans are slow (on the order of 10 min. each). In order to maintain stability during USAXS scans, the temperature was held constant, leading to the step-wise nature of the temperature cycle. Scans were also collected at intermediate temperatures on LX-17, but simply showed behavior intermediate to the temperature extremes. Scans at room temperature are important to determining the irreversible damage (i.e. not simply thermal expansion or contraction) and are collected between the two temperature extremes.

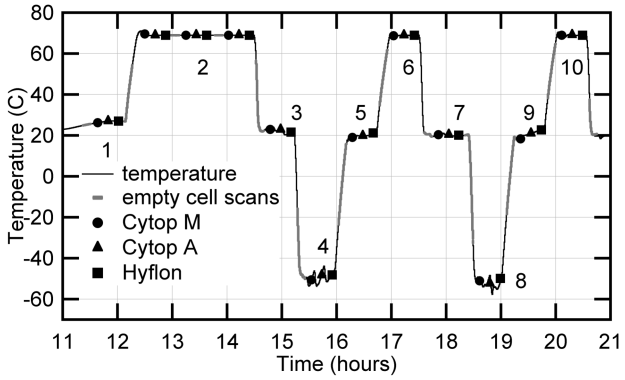

Figure 2: Temperature vs. time for Cytop M, Cytop A, and Hyflon binders. The LX-17 and UFTATB samples underwent similar temperature cycling. The numbers correspond to the traces listed in Fig. 3.

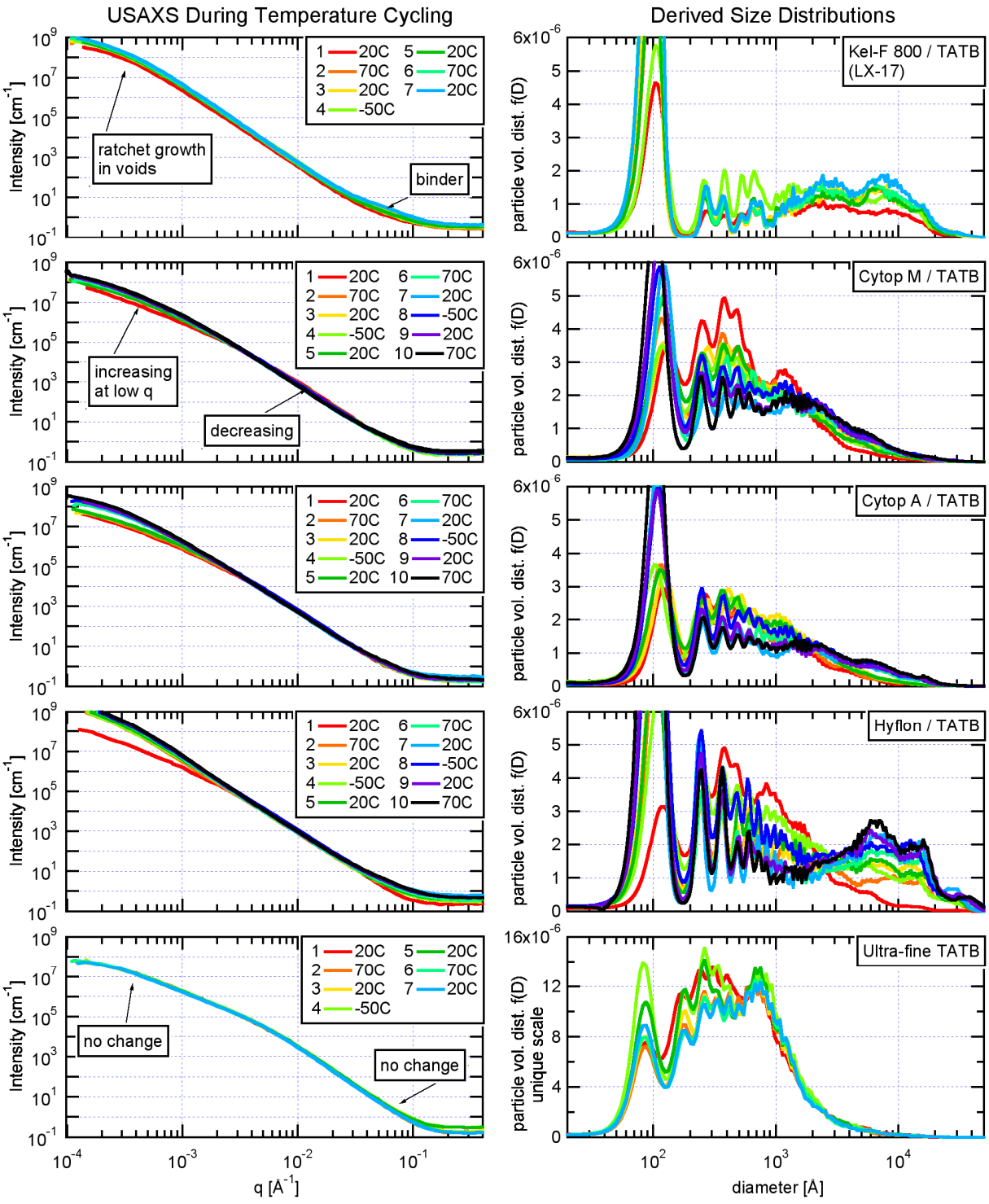

Figure 3: Left panes: USAXS during temperature cycling for the 5 different samples. The traces are numbered in the acquisition order; the corresponding times and temperatures are presented in Fig. 2 for the middle three samples Cytop M, Cytop A, and Hyflon. Right panes: Maximum entropy derived USAXS size-distributions (consistent color scheme with left panes). Note the different y-axis scale for UFTATB size distributions.

Figure 3 presents the slit-desmeared USAXS data in the left panes, and the maximum-entropy derived size distributions in the right panes. LX-17 appears in the top panes, while ultra-fine TATB appears in the bottom panes. Cytop M, Cytop A, and Hyflon appear in rows 2, 3 and 4, respectively. All of these explosive formulations have a power-law slope very close to -4: in the top three samples with binder in the region from about 5×10^{-3} to about 2×10^{-2} Å^{-1}; while in UFTAB, this occurs about 1×10^{-2} to about 4×10^{-2} Å^{-1}. These -4 slopes indicate the larger scatterers (~100 nm to ~1 μm) are three dimensional (for example, spherical) rather than 2-dimensional (disk-like) or 1-dimensional (rod-like). Further, this indicates a smooth, sharp, and abrupt interface, rather than a rough, fractal-like surface of the pores.

Temperature-dependent changes in the raw USAXS (left panes) are immediately apparent. LX-17, the top panes in Figure 3 exhibit "ratchet-growth" as is seen in the increase in the scattering intensity ~ 3×10^{-4} Å^{-1}, and both a shift of the distribution of voids to both larger size and higher occurrence depicted in the top right pane. The USAXS scans before and after the temperature cycle resemble results of previous, ex-situ measurement of the void changes[11]. The USAXS-derived void volume (~ 1 nm to ~ 2 μm) for the LX-17 is 1.4% before the temperature cycles, and increases to 3.5 % after the cycling.

The irreversible changes occur during the warm portion of the temperature cycle. Figure 4 presents a close-up of the Gunier region of the USAXS, corresponding to structures ~ 1 micron in size. Only room temperature scans are shown for two complete temperature cycles. Minimal changes to the USAXS occur after cold cycles, while much larger changes occur after warm cycles. This indicates the actual changes to the voids in the material occur at warm temperatures.

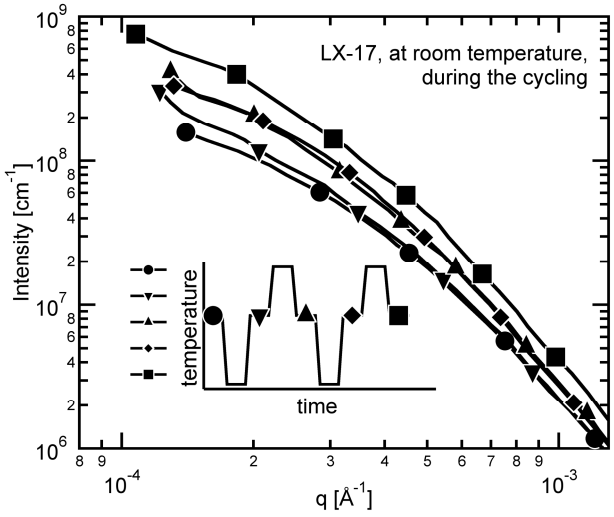

Figure 4: USAXS profiles at room temperature throughout the temperature cycle, region where voids ~ 1 micron would affect the Gunier region. The inset graphically indicates the acquisition time as follows: circles: before cycling; downward-pointing triangles: after the first cold cycle; upward-pointing triange: after a cold and hot cycle; diamonds: after a cold, hot, and cold cycle; and boxes: after cold, hot, cold and hot cycles.

Note much greater changes to the USAXS after hot cycles: the irreversible growth occurs primarily during warm cycles rather than cold.

The three middle rows of Figure 3 present the TATB formulations using Cytop M, Cytop A, and Hyflon binders. Some of these new test formulations perform well during temperature cycling compared to TATB/Kel-F 800 composites; results of void volume derived from the USAXS appear in Table 1. First, the voids measurable with USAXS are only 0.9% and 0.6% in the freshly pressed TATB/Cytop M and TATB/Cytop A. In these two cases, the mean pore size is smaller than in TATB/Kel-F 800 explosives. During temperature cycling, these two materials expand in either the first or second cycle, and then show reduced expansion over subsequent cycles. It is also clear that voids are experiencing some type of coalescing behavior. In the USAXS (especially in the second row, left pane) a reduction in scattering intensity is seen at $q \sim 10^{-2}$ Å^{-1} with a corresponding increase of intensity at lower q ($\sim 10^{-4}$ Å^{-1} to 10^{-3} Å^{-1}). The derived size distributions as well as the mean size are clearly moving towards larger size. However, even after temperature cycling, these two new explosives exhibit 1.3% and 1.1% void volume measured with USAXS in TATB/Cytop M and TATB/Cytop A respectively. These values are typical for or even better than porosity found in TATB/Kel-F 800 explosives before temperature cycling. The final Hyflon binder did not perform as well as LX-17 under temperature cycling. The void volume increased from 1.6% to 4.6% over only a few temperature cycles. Note the excessive amount of voids ~ 1 μm appearing during the cycling in this Hyflon-based sample.

Table 1. Changes to void volume derived from the USAXS; sensitive from about 10 nm to about 2-3 microns.

Sample	Before cycle	After cycle
LX-17 (Kel-F 800 / TATB)	1.4%	3.5%
Cytop M / TATB	0.9%	1.3%
Cytop A / TATB	0.6%	1.1%
Hyflon AD60 / TATB	1.6%	4.6%
Ultra-fine TATB (no binder)	2.2%	2.1%

In contrast to PBX formulations of TATB, mesoscale structure of UFTATB measured by USAXS shows insignificant changes during temperature cycling. This striking result is demonstrated by the USAXS at each temperature, as seen in the bottom left pane of figure 3. Scans at various times during the temperature cycle lie nearly perfectly on top of one another for $q < 5 \times 10^{-2}$ Å^{-1}. Voids ~100 nm to ~ 1 um, seen in the size distributions derived via maximum-entropy in the lower right pane, are not changing. UFTATB shows, within the sensitivity of USAXS, about 2.2% void volume before, and 2.1% after, essentially the same void volume

within the error of this measurement. Thus, any changes to porosity in UFTATB during temperature cycling are occurring at sizes larger than about 2 microns. Ratchet growth in voids important to hot-spot models (~100nm - ~1um) is highly dependent upon the binder and potentially dependent upon TATB crystallite size.

In addition to ratchet growth, the intensity increase seen at relatively high scattering angle ($q \sim 5 \times 10^{-2}$ Å^{-1}) at warm temperatures is very slight in the UFTATB case compared to the formulated explosives using Kel-F 800 as a binder. Although we previously attributed this scattering to structure intrinsic to the TATB crystallites[15], significant changes are occurring in this ~10 nm size regime in PBX formulations in addition to scattering caused by intrinsic TATB porosity. It thus appears that the binder plays a strong role in observed changes in structure occurring at the ~10 nm scale during temperature cycling. In LX-17, this could be due to nanoscale bubble formation in the Kel-F 800 at 70C, or at least partly due de-crystallization of the polymer above the glass transition temperature of the Kel-F. USAXS is optimized for $q \sim 10^{-4}$ Å^{-1} to 10^{-1} Å^{-1}, and while $q \sim 1$ Å^{-1} can be reached, the background seen in these materials becomes significant above 10^{-1} Å^{-1}. Thus, to investigate these tiny 10 nm structures, standard SAXS would be a better alternative. The Cytop M, Cytop A, and Hyflon binders support the hypothesis that these small scatters are due to the binder. First, explosives formed with Cytop M and Cytop A binders exhibit detectable but minimal changes at scattering angles corresponding to structures ~10 nm. In the third case, the Hyflon binder shows an increase by a factor of 6.7, somewhat comparable to LX-17, where in this particular case, an increase by a factor of 4.3 was observed over the first few temperature cycles. Thus, the degree of change seen in this peak is highly binder-dependent, and essentially absent in binder-less systems. We thus hypothesize that along with relatively static intrinsic pores (as observed in UFTATB) the changes in scattering at $\sim 5 \times 10^{-2}$ Å^{-1} are due to delamination of the binder with the TATB, or cavitation within the binder. Note that in all of the right panes of Fig. 3, but especially prominent in the Hyflon sample after temperature cycling, an intense ~10 nm peak in a derived size distribution leads to short-period oscillations at about 20 - 80 nm diameter. These oscillations are artifacts due to maximum entropy fitting of the large amount of scatterers about 10 nm.

3.2 Theory and Modeling

Many of the important results presented above can be understood on the basis of: (1) strength and quality of polymer-TATB binding; (2) glass-transition temperature (T_g) of the binder employed; and (3) irreversible displacement of particles (i.e. TATB crystallites) due to anisotropic stress fields generated by thermal expansion of individual particles, especially at $T > T_g$. As for polymer-TATB binding, we have carried out atomic level molecular dynamics (MD) simulations[1] to compute the work of adhesion (W) and the spreading coefficient (S) of various binders on two prominent TATB facets, i.e., the [001] facets, coplanar to the TATB molecules, and [100] facets, coplanar to edges of TATB molecules. Results are listed in Table 2. Given that in our sign convention it is desirable to have both W and S to be large and positive for all exposed TATB facets, the deficiency of Hyflon at the [001] facet becomes immediately apparent from Table 2. This ineffectiveness could be explained by examining the differences in Fluorine-density-profiles of the different binders at the TATB interface[1].

Table 2: Work of adhesion (*W*) and spreading coefficient (*S*) for the two prominent TATB facets [001] and [100] computed by atomistic MD simulations. All units are in *erg/cm^2*.

Binder	Interface [001]		Interface [100]	
	W	*S*	*W*	*S*
Kel-F 800	+76	+22	+271	+217
Cytop	+87	+39	+275	+227
AF	+78	+37	+281	+235
Hyflon	+5	-39	+320	+276

In order to obtain deeper insight into the mechanism behind ratchet growth in our TATB-PBX, we have recently developed a mesoscale model in which a coarse-grained (micron-scale) interaction Hamiltonian was derived for such systems[16, 17]. This model allowed a quantitative reproduction of experimentally observed irreversible growth through explicit molecular dynamics simulations. In the process we also identified a critical interaction parameter of our model that has a strong correlation with binder properties.

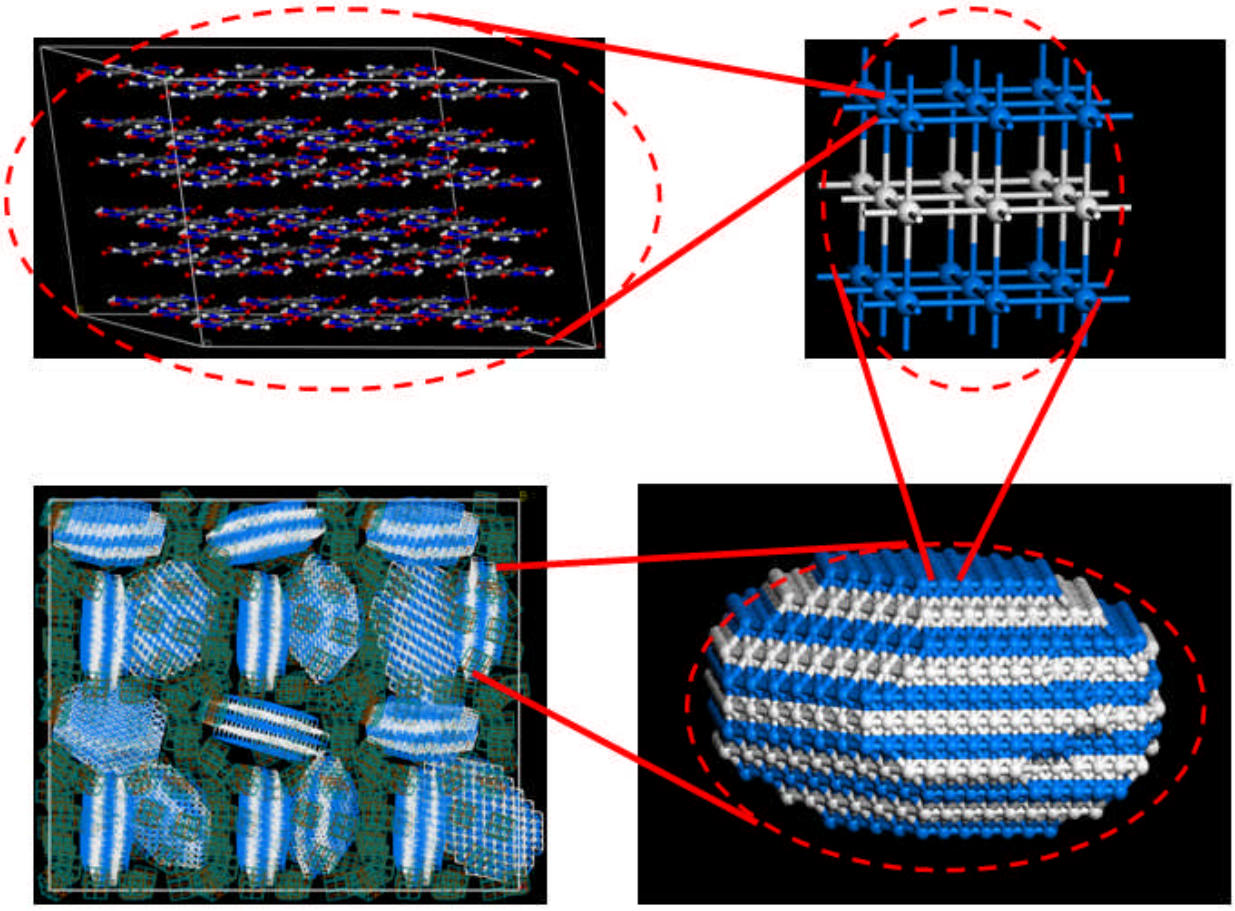

Figure 5: Mesoscale model of TATB powder. (clockwise from top left): atomistic model of TATB crystal; a single TATB crystal defined in terms of micron-scale "beads". Two different bead-types are defined in order to incorporate anisotropy, i.e., to distinguish between "in-plane" and "normal toplane"; a single TATB "particle" or "crystallite" with shape similar to that predicted from equilibrium morphology; and a representative model of a "powder" consisting of TATB particles of different sizes packed with small particles in order to achieve experimental packing density. See references [16] and [17] for more details.

Our mesoscale MD simulations lead to the following picture: First, ratchet growth happens by the movement of crystallites induced by anisotropic stress build up due to intrinsic crystalline anisotropy. In the isotropic case, all crystallites expand by the same fractional amount in all directions, and there is little residual stress that can drive volume growth. Anisotropy-generated local stress, in contrast, tends to drive crystallites from an initial pressed-powder configuration to one of a large number of metastable states with slightly less compaction density, but likely with higher configurational entropy. In the absence of small particles, such a movement gets jammed due to facetted morphology of the large crystallites, while the presence of the former effectively act as lubricants and allow the system to move out of the compacted geometry and explore the metastable phase space. The small particles are either present in the original powder sample, or are created during the pressing process to high compaction density. Second,

the above displacement of particles becomes prominent in Kel-F 800 based materials only at a temperature above the binder T_g, when the binder itself flows, with significant loss of binding strength. This would clearly explain why ratchet growth and new void creation in our experiments are seen only at elevated temperatures in Kel-F 800 based materials. It is also consistent with why Cytop, with a much higher T_g than Kel-F 800, impedes ratchet growth much more effectively. This is not the only parameter controlling ratchet growth. The Hyflon T_g is similar to Cytop, but does not inhibit ratchet growth, in fact, this material performs worse than Kel-F 800, which has a much lower T_g. In this case, the poor wetting and ahesion properties of this material on the [001] facet of TATB presumably lead to delamination of Hyflon from TATB, leading to ratchet growth. Third, void creation, merging, and redistribution can all be tied to the displacement of TATB particles, both large and small, as well as defect (i.e. new void) creation within the binder itself. Our mesoscale MD model, as it currently stands, only allows the study of particle displacements. Analysis of such displacements in our simulations is consistent with the creation and merging of voids within a length-scale spanning a few tens of nm to a few microns, clearly in the range of our experimental observations (see Figs. 3 and 4).

4 Conclusions

UFTATB, LX-17, and formulations using Cytop M, Cytop A, and Hyflon AD60 polymer binders have been studied during temperature cycling between -55º C and 70º C. Multiple lots of LX-17 show the same behavior: an increase in size and number of voids as the temperature is cycled, and the dramatic appearance of x-ray scattered at angles corresponding to structures ~ 10 nm when the explosive is heated. UFTATB does not show a significant increase in these smaller structures, inferring that the additional intensity is due to changes associated with the Kel-F 800 binder. Supporting this result, Hyflon also has drastic changes, while the two Cytop binders, computed to have good TATB adhesion properties, and possessing high glass-transition temperature, show only a slight increase in 10 nm structures. These Cytop binders control ratchet growth better than LX-17 for changes in voids ~100 nm to ~ 1 μm: LX-17 in this work shows an increase in the volume due specifically to structures of this size from 1.4% to 3.5%; while PBXs using the Cytop binders showed increases from 0.85% to 1.3% and 0.6% to 1.1%. A third binder, Hyflon, did not perform as well as LX-17, with an increase from 1.2% to 4.6% after two temperature cycles. Amazingly, UFTATB shows no change in void volume or void distribution between ~ 100 nm and ~1 μm. Any volume expansion seen in this material during ratchet growth is due to formation of porosity with dimensions larger than a few microns. These results are consistent with, and can be explained, by two models. First, atomistic calculations show that Hyflon has poor adhesion to TATB, and experimental evidence is that delamination between binder and TATB occurs, leading to excessive ratchet growth. Second, a mesoscale model explains many of the observed features, including the role of crystalline anistotropy of TATB and the effect of binders on ratchet growth. It also provides a mechanistic understanding of ratchet growth in terms of particle displacements, and provides useful insight into the resulting creation and merging of voids at experimentally observed length-scales. These results demonstrate that both TATB adhesion and high glass-transtion temperature are important to minimizing changes to voids ~100 nm to ~1 micron and controlling ratchet growth.

5 References

[1] R. H. Gee, A. Maiti, S. Bastea and L. E. Fried, Molecular dynamics investigation of adhesion between TATB surfaces and amorphous fluoropolymers. *Macromolecules*, **2007**. *40*(9), 3422-3428.

[2] J. L. Maienschein and F. Garcia, Thermal expansion of TATB-based explosives from 300 to 566 K. *Thermochimica Acta*, **2002**. *384*(1-2), 71-83.

[3] P. Lewis, B. Cunningham, S. D. Teresa, P. Harwood and T. Tran, Density Variations in IHE Formulations Due to Thermal Cycling. *Lawrence Livermore National Laboratory Report, UCRL-JC-147462*, **2002**.

[4] J. R. Kolb and H. F. Rizzo, Growth of 1,3,5-Triamino-2,4,6-Trinitrobenzene (Tatb) .1. Anisotropic Thermal-Expansion. *Propellants, Explosives, Pyrotechnics*, **1979**. *4*(1), 10-16.

[5] R. H. Gee, S. Roszak, K. Balasubramanian and L. E. Fried, Ab initio based force field and molecular dynamics simulations of crystalline TATB. *Journal of Chemical Physics*, **2004**. *120*(15), 7059-7066.

[6] H. F. Rizzo, J. R. Humphrey and J. R. Kolb, Growth of 1,3,5-Triamino-2,4,6-Trinitrobenzene (Tatb) .2. Control of Growth by Use of High Tg Polymeric Binders. *Propellants and Explosives*, **1981**. *6*(2), 27-36.

[7] H. F. Rizzo, J. R. Humphrey and J. R. Kolb, Growth of 1,3,5-Triamino-2,4,6,-Trinitrobenzene (Tatb) .2. Control of Growth by Use of High-Tg Polymeric Binders. *Propellants and Explosives*, **1981**. *6*(3), 57-62.

[8] Y. A. Vlasov, V. B. Kosolapov, L. V. Fomicheva and I. P. Khabarov, Effect of temperature, density, and technical factors on the shock-wave sensitivity of plastic TATB. *Combustion Explosion and Shock Waves*, **1998**. *34*(4), 467-469.

[9] R. Belmas, A. Bry, C. David, L. Gautier, A. Keromnes, D. Poullain, G. Thevenot, C. Le Gallic, J. Chenault and G. Guillaumet, Preheating sensitization of a TATB composition part one: Chemical evolution. *Propellants Explosives Pyrotechnics*, **2004**. *29*(5), 282-286.

[10] P. A. Urtiew, C. M. Tarver, J. L. Maienschein and W. C. Tao, Effect of confinement and thermal cycling on the shock initiation of LX-17. *Combustion and Flame*, **1996**. *105*(1-2), 43-53.

[11] J. C. Dallman and J. Wackerle. Temperature-Dependent Shock Initiation of TATB-based High Explosives. in Proceedings of the 10th International Detonation Symposium. 1993. Boston, MA.

[12] R. Belmas and J. P. Plotard, Physical Origin of Hot-Spots in Pressed Explosive Compositions. *Journal De Physique Iv*, **1995**. *5*(C4), 61-87.

[13] C. M. Tarver, S. K. Chidester and A. L. Nichols, Critical conditions for impact- and shock-induced hot spots in solid explosives. *Journal of Physical Chemistry*, **1996**. *100*(14), 5794-5799.

[14] Y. Hamate and Y. Horie, Ignition and detonation of solid explosives: a micromechanical burn model. *Shock Waves*, **2006**. *16*(2), 125-147.

[15] T. M. Willey, J. Handly, B. L. Weeks, T. v. Buuren, J. Ilavsky, J. R. I. Lee, G. E. Overturf and J. H. Kinney, Changes in Pore Size Distribution upon Thermal Cycling of TATB-

based Explosives Measured by Ultra-Small Angle X-ray Scattering. *Propellants, Explosives, Pyrotechnics*, **2006**. *31*(6), 466-471.
[16] R. H. Gee, A. Maiti and L. E. Fried, Mesoscale modeling of irreversible volume growth in powders of anisotropic crystals. *Applied Physics Letters*, **2007**. *90*(25), 254105.
[17] A. Maiti, R. H. Gee, D. M. Hoffman and L. E. Fried, *Journal of Applied Physics*, **2008**. *in press*.
[18] R. J. Roe, Methods of X-ray and Neutron Scattering in Polymer Science. Topics in Polymer Science: A Series of Advanced Textbooks and Monographs, ed. J. E. Mark. 2000: Oxford University Press. 331.
[19] O. Glatter and O. Kratky, Small Angle X-ray Scattering. 1982, Academic Press Inc.: London. p. 515.
[20] P. R. Jemian, Characterization of Steels by Anomalous Small-angle X-ray Scattering, in Materials Science and Engineering. 1990, Northwestern University: Evanston, IL. p. 222.
[21] J. Ilavsky and P. R. Jemian, Irena and Indra SAXS data analysis macros, including Maximum Entropy. 2008.
[22] J. A. Potton, G. J. Daniell and B. D. Rainford, A New Method for the Determination of Particle Size Distributions from Small-angle Neutron Scattering Measurements. *Journal of Applied Crystallography*, **1988**. *21*, 891-897.
[23] J. A. Potton, G. J. Daniell and B. D. Rainford, Particle Size Distributions from SANS Data Using the Maximum Entropy Method. *Journal of Applied Crystallography*, **1988**. *21*, 663-668.
[24] J. Ilavsky, A. J. Allen, G. G. Long and P. R. Jemian, Effective pinhole-collimated ultrasmall-angle x-ray scattering instrument for measuring anisotropic microstructures. *Review of Scientific Instruments*, **2002**. *73*(3), 1660-1662.
[25] J. Ilavsky, P. R. Jemian, A. J. Allen and G. G. Long, Versatile USAXS (Bonse-Hart) Facility for Advanced Materials Research. *8th International Conference on Synchrotron Radiation Instrumentation (SRI 2004), AIP Conference Proceedings*, **2004**. *705*, 510-513.
[26] G. G. Long, A. J. Allen, J. Ilavsky, P. R. Jemian and P. Zschack, The Ultra-Small-Angle X-ray Scattering Instrument on UNICAT at the APS. *Synchrotron Radiation Instrumentation: 11th U.S. National Conference, AIP Conference Proceedings*, **2000**. *521*, 183-187.
[27] J. Ilavsky, D. Shu, P. Jemian and G. Long, Versatile collimating crystal stage for a Bonse-Hart USAXS instrument. *9th International Conference on Synchrotron Radiation Instrumentation (SRI 2006), AIP Conference Proceedings*, **2007**. *879*, 1833-1836.

Acknowledgments

We acknowledge funding from project 06-SI-005 of the Laboratory Directed Research and Development Program at LLNL. This work was performed under the auspices of the U.S. Department of Energy by Lawrence Livermore National Laboratory under Contract DE-AC52-07NA27344. Use of The Advanced Photon Source is supported by the U. S. Department of Energy, Office of Science, Office of Basic Energy Sciences, under Contract No. DE-AC02-06CH11357.

Symbols and Abbreviations

TATB	1,3,5 triamino-2,4,6-trinitrobenzene
USAXS	Ultra-small angle x-ray scattering
Kel-F 800	Fluoropolymer binder, vinylidene fluoride-chlorotrifluoroethylene copolymer
LX-17	A polymer-bonded explosive using 92.5% TATB, 7.5% Kel-F 800
UFTATB	Ultra-fine TATB
Cytop M	Commercially available polymer; see ref. [1]
Cytop A	Commercially available polymer; see ref. [1]
Hyflon AD60	Commercially available polymer; see ref. [1]
PBX	Polymer-bound explosive or plastic-bonded explosive

LLNL-JRNL-401946